UNDERSTANDING HYDROGEN EMBRITTLEMENT OF FRACTURE TOUGHNESS TESTED LINE-PIPE STEELS USING FRACTOGRAPHY & MACHINE LEARNING TECHNIQUES

Tuhin Das*, John Vande Voorde, Nuria Sanchez
ArcelorMittal Global Research and Development (OCAS N.V.), Pres. J.F. Kennedylaan 3, 9060 Zelzate, Belgium

Nikolaos Voudouris, Sofia Rapti, Athanasios Tazedakis
Corinth Pipe Works (CPW) Research & Development, VI.PE. Thisvis, 320 10 Domvrena Viotia, Greece

Frederic Bouchaud
ArcelorMittal Europe, Customer Technical Support Energy Pipes, Batiment L9, 13776 Fos-sur-Mer, France

ABSTRACT

Hydrogen embrittlement (HE) presents a significant challenge to the integrity of line-pipe steels, particularly in applications involving the transport and storage of hydrogen gas. As a result, understanding the impact of hydrogen on the fracture behaviour of line-pipe steels is essential for the safe deployment of hydrogen infrastructure. The current study dives into the HE mechanisms of pipeline steels in high-pressure H_2 environment leveraging multiple techniques. For this purpose, fracture toughness tests of compact tension (CT) specimens of industrial grade line-pipe steels (coils and pipes) were performed at 100 bar at CPW's hydrogen laboratory, using the reversing direct current electric potential difference (DCEPD) method to enable a real time crack initiation and crack growth measurement.

Based on the relative fracture toughness performances, a pair of coils (Coil A & Coil B) and pipes (Pipe X & Pipe Y) were selected for fracture surface mapping, advance characterization and machine learning (ML) technique. A detailed fracture surface mapping of the coils and pipes reveal that their fracture morphology is affected by HE when tested at 100 bar H_2 compared to the ductile dimple morphology of their air tested counterparts. Several out-of-plane "secondary cracks", *perpendicular* to the primary crack propagation direction were observed both in the stretch zone (or boundary) and crack extension zone in the fracture surface. Coil B, however, exhibited large out of plane "groove cracks", *parallel* to the direction of primary crack propagation in the crack extension zone. These grooves could be associated with aligned microstructural features such as segregation bands, banded structures with weak phase boundaries, non-metallic inclusions (NMIs) or crystallographic texture. A good correlation was observed between the fracture toughness results and the stretch zone morphology and secondary cracks. For instance, the stretch zone in Pipe X (with higher fracture toughness) shows a clear planar transition between the fatigue pre-crack and crack extension zone. On the other side, the stretch zone in the Pipe Y is vanishingly small showing an entirely flat surface with multiple large secondary cracks. An advance postmortem analysis into the mechanism(s) of the secondary crack formation reveal that these cracks are associated with hydrogen enhanced dislocation activity just underneath fracture surface, leading towards hydrogen enhanced localized plasticity (HELP) mechanism. A quantitative comparison of the total secondary crack area using a ML approach rooted in computer vision that higher secondary crack area corresponds to lower crack growth resistance in the materials. Nevertheless, the secondary cracks could be relatively less detrimental compared to the groove cracks as far as the crack growth resistance performance is considered in high pressure H_2 environment.

DISCLAIMER

1. INTRODUCTION

The global energy transition necessitates a significant shift towards hydrogen as a clean energy carrier. Alongside pure H_2 transportation, the energy sector is actively investigating the practicality of blending H_2 with natural gas, a strategy that seeks to leverage existing pipeline infrastructure to reduce carbon footprints associated with energy delivery in a cost-effective way. This approach is seen as a rapid pathway toward large-scale hydrogen energy implementation along with the establishment of new line-pipe infrastructures in EU and around the globe, as stated in a recent International Energy Agency (IEA) report [1].

Despite hydrogen's promise, its transport poses serious material integrity challenges. Hydrogen embrittlement (HE) is a major concern for line-pipe steels, presenting considerable risks to structural integrity. Hydrogen is known to substantially diminish the fatigue and fracture resistance of these steels, necessitating the application of conservative operating conditions and large safety factors in current practices for H_2 storage and distribution. Therefore, a comprehensive understanding of the fracture characteristics of steel grades used in pipelines is indispensable for ensuring safe and reliable design and operation. Fracture toughness of line-pipe steels in H_2 environment is influenced by several factors, such as, microstructure, yield strength, H_2 pressure, charging conditions (in-situ, pre-charged), etc. For instance, higher-strength steels generally exhibit a more pronounced decrease in fracture toughness and are susceptible to HE at lower H_2 pressures [2]. The microstructure of line-pipe steels is known to play a critical role in affecting their fracture toughness fatigue properties in H_2 environments [3]. Different microstructures, such as ferritic-pearlitic and bainitic, influence how hydrogen interacts with the steel, and where cracks initiate and propagate. Despite extensive research efforts, a comprehensive understanding of HE in line-pipe steels at the micro and nanoscale remains elusive due to their inherent microstructural complexities. It indicates that while macroscopic effects of HE is somewhat well-documented, the fundamental, atomistic interactions of hydrogen with specific microstructural features (e.g., dislocations, inclusions, phase interfaces, etc.) and their precise manifestation in mechanical degradation are still not fully elucidated. It is even more elusive when design critical mechanical tests are considered. Evaluation methodology of HE in gaseous H_2 environment based on fracture toughness tests are still evolving while fundamental understanding of the synergistic interactions of stress, hydrogen and microstructure is still missing. This is a critical gap because microstructural engineering alongside suitable HE evaluation criteria represents a key pathway not only to qualify the current materials but also to develop next-generation pipeline steels for H_2 applications. Therefore, an approach underscoring the postmortem analysis has been adopted here to bridge the gap and advance knowledge towards this direction. For this purpose, fracture toughness tests of compact tension (CT) specimens of industrial grade line-pipe steels (coils and pipes) were performed following ASTM E1820-22 [4] and CSA CHMC 1-2014 [5] at 100 bar. Following the fracture toughness performances, a pair of coils (Coil A & Coil B) and pipes (Pipe X & Pipe Y) were utilized for fracture surface mapping, advance characterization and machine learning (ML) technique. A detailed fracture surface mapping was performed to study the stretch and crack extension zones identifying the different modes of fracture. Two different types of out-of-plane crack formation were observed, i.e., "secondary cracks" *perpendicular* to the primary crack propagation direction and, "groove cracks" *parallel* to the direction of primary crack propagation. The groove cracks were observed in the crack extension zone of Coil B, exclusively. However, the secondary cracks were observed both in the stretch zone (or boundary) and crack extension zone of the other materials. The presence or area coverage of those cracks varied among the materials in correlation with the toughness results. For instance, the stretch zone in Pipe X (with higher fracture toughness) shows a clear planar transition between the fatigue pre-crack and crack extension zone with very fine secondary cracks. On the other side, the stretch zone in the Pipe Y is vanishingly small showing an entirely flat surface with multiple large secondary cracks. The potential origin of this secondary crack formation was studied in relation to microstructural evolution by taking focused ion beam (FIB) lift-outs just beneath the fracture surface. The advanced postmortem analysis indicates that that these cracks are associated with hydrogen enhanced dislocation activity revealing high density of dislocation cell formation around those cracks. Furthermore, a quantitative assessment of the total secondary crack area using a ML approach reveals that higher secondary crack area corresponds to lower crack growth resistance in the materials.

2. METHODOLOGY

2.1. Fracture toughness testing

Rising Load Fracture Toughness Testing was performed as per ASTM E1820-22, at Corinth Pipe Works's (CPW's) hydrogen autoclave laboratory using 100% hydrogen gas with a purity of 6.0 at 100 bar and ambient temperature. To achieve a pure H_2 environment, a rigorous purging protocol was implemented including multiple pressurization and depressurization cycles, initially with inert gases such as nitrogen, followed by sequential high-purity hydrogen replenishments. Tests with a monotonically increasing stress intensity, i.e., K-rate of 0.1 MPa√m/min (recommended range in CSA CHMC 1-2014 standard) was used to determine the threshold fracture toughness from J-integral vs. crack extension (J-R) curves.

Standard compact tension (CT) specimens were prepared as per ASTM E1820 Annex A2 (Fig. 1 (a)), with a thickness (B) of 12.7 mm (0.5") and width-to-thickness (W/B) ratio of 4. Orientation of the CT specimens w.r.t the parent material is shown in Fig. 1 (b). The specimens were side grooved with a reduction of 0.20B (10% per side) and groove root radius of 0.5 ± 0.2 mm, with an included angle below 90°. Side grooves were introduced after fatigue pre-cracking, with the groove root aligned along the specimen centreline ensuring symmetry. Fatigue pre-cracking was conducted in air using a crack mouth opening displacement (CMOD) extensometer such that the pre-crack depth is at least 0.1B or 1 mm (whichever was greater). The final normalized crack length (a_0/W) was maintained at 0.45-0.55 ensuring valid fracture toughness measurements. CMOD was controlled via an actuator and measured using Linear Variable Differential Transformer (LVDT) sensors.

Crack growth was monitored using the reversing direct current electric potential difference (DCEPD) method. The plastic deformation effects were isolated using a reference DCEPD signal (V_o) at the onset of ductile crack extension. Subsequent changes in the DCEPD signal quantified crack growth beyond this point. The extent of ductile crack extension was determined through combined analysis of CMOD vs. DCEPD and force vs. DCEPD plots, providing the basis for constructing the J–R curves.

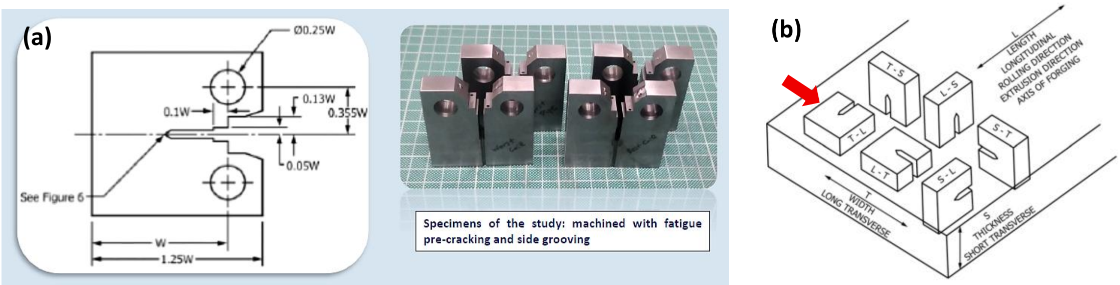

Fig. 1: (a) CT specimen geometry, (b) CT sample orientation marked by red arrow.

2.2. Characterization

All the characterization activities were performed at OCAS using in-house characterization facilities. Fractography and fracture surface mapping were performed using a scanning electron microscope (SEM) equipped with W filament electron source for secondary electron (SE) imaging with information on the morphology, backscattered electron (BSE) imaging and, energy dispersive detection of characteristic X- rays of the analysed surface for qualitative detection of elements.

Image generation by (scanning) transmission electron microscopy (STEM) is based on the interaction of a high energy electron beam with a thin sample. (S)TEM in OCAS is equipped with four in-column energy dispersive X-ray (EDX) detectors having a spatial resolution of 0.1 nm, that allows for high-resolution TEM and STEM imaging with fast navigation for dynamic microscopy and precise EDX analysis in all dimensions. TEM samples (FIB lamellae) of <200 nm thickness were prepared using a dual-beam focused ion beam system that incorporates both focused ion beam (FIB) for site-specific material removal and non-destructive SEM imaging.

3. RESULTS

3.1. General characterization

All materials for this research were industrially produced by ArcelorMittal Europe as hot-rolled coils with varying thicknesses, following the thermomechanical controlled processing (TMCP) route to obtain the targeted microstructure and mechanical properties. The coils were then used to manufacture pipes at the pipe mills of CPW, of required diameter. However, for this exercise and other research activities, a set of samples/coupons were sectioned from "Coil A" and "Coil B" before pipe manufacturing, while the other set of samples/coupons were obtained from the HFI pipes directly as "Pipe X" and "Pipe Y". The outer diameters of the Pipe X and Pipe Y are 26" and 16", respectively. The overall microstructure of the low carbon steel samples is bainitic ferrite type, with similar phase fraction of pearlite and cementite, and comparable grain sizes. However, the cleanliness index of Coil B is double compared to Coil A. Based on the evaluation methodology described in ISO 4967 (method B, appendix C) [6], a lower cleanliness index represents lower presence of inclusions, i.e., a cleaner steel. The cleanliness indices for Pipe X and Pipe Y are somewhat comparable. The general properties for the coil and pipe samples are summarized in Table 1. HE indices in terms of percent elongation $\left(\frac{El_{air}-El_H}{El_{air}} \times 100\right)$, from the *in-situ* slow strain rate tensile (SSRT) tests are also provided in Table 1. Coil B and Pipe Y are more susceptible than Coil A and Pipe X, respectively. Initially, the SSRT tests were performed on a set of Coils and Pipes to select a pair of coils (Coil A & Coil B) and pipes (Pipe X & Pipe Y), for fracture toughness tests in 100 bar H_2. The results from the fracture toughness tests will follow in the next section.

Material	Thickness (mm)	Outer diameter (in.)	P_{cm}	Yield strength, YS (MPa)	YS/TS	HE_{EL}(%) (SSRT test)
Pipe X	15.9	26	0.15	498	0.81	29
Pipe Y	19.1	16	0.15	538	0.91	31
Coil A	16	--	0.16	555	0.87	15
Coil B	20.6	--	0.16	601	0.9	27

Table 1: Properties of pipes and coils

3.2. Fracture toughness

The fracture toughness measurements for the pipes and coils evaluated following the ASTM E1820-22 and CSA CHMC 1-2014, are listed in Table 2. Fracture toughness at 100 bar H_2 was evaluated with a monotonically increasing stress intensity with a K-rate of 0.1 MPa√m/min, while the tests in air were performed with a K-rate of 3.8 MPa√m/min. The fracture toughness results in Table 2 suggest that all four materials are somewhat susceptible to HE and suffers mechanical performance degradation in H_2 environment. Nevertheless, the performance of all the materials comfortably qualifies the toughness requirements as per the ASME B.31.12 design code [7], for H_2 pipeline usage. However, it is imperative that Coil A performs better than Coil B while Pipe X performs better than Pipe Y in the same H_2 environment, corroborating with the evaluations from the SSRT tests.

It can be noticed that if the onset fracture toughness value is considered, i.e., K_{Jth}, there is no significant difference between air and H_2 tested conditions. Clearly, the acceptance of $K_{JQ0.2}$ (evaluated from elastic-plastic fracture toughness, $J_{Q0.2}$) as the fracture toughness distinguishes between the two different environmental conditions, similar to the observation made in the DNV H2PIPE JIP report [8]. It should be also noted that the fracture toughness values inversely correlate with the yield strength (Table 1) of the corresponding coils and pipes. Materials with relatively lower yield strength show better performance in H_2, with respect to fracture toughness. The inverse relationship between the fracture toughness and yield strength of a line pipe steel, has been widely suggested in literature [2]. And our evaluations are no exception, thus, also suggesting the competency of the evaluation set-up and methodology even when the differences (in yield strength) are not very significant. However, fundamental understanding of the fracture behaviour is necessary to develop next generation H_2 ready pipeline steels. Therefore, further investigations have been carried in the following sections.

Material	Environment	Fracture toughness, $K_{JQ0.2}$ (MPa√m)	Additional measurements		
			$J_{Q0.2}$ (kJ/m^2)	J_{th} (kJ/m^2)	K_{Jth} (MPa√m)
Pipe X	Air	--	--	--	--
	H_2 (100 bar)	116	59	48	104
Pipe Y	Air	182	145	35	89
	H_2 (100 bar)	91	36	27	79
Coil A	Air	194	165	50	106
	H_2 (100 bar)	118	61	43	99
Coil B	Air	189	158	25	75
	H_2 (100 bar)	77	26	21	69

Table 2: Fracture toughness properties of pipes and coils

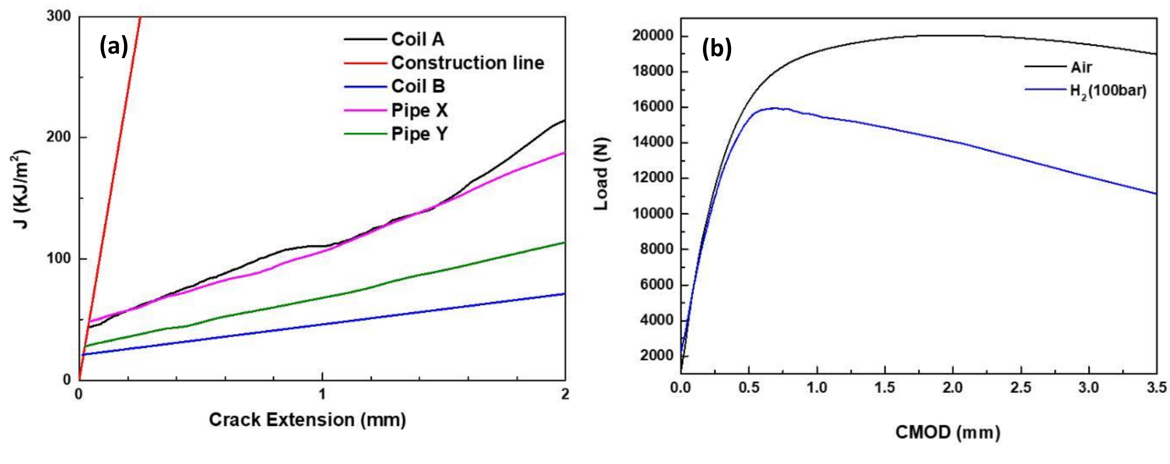

Fig. 2: (a) J-integral vs. crack extension (J-R) curves for all the materials in 100 bar H_2. (b) Load vs crack mouth opening displacement (CMOD) plots in air and 100 bar H_2 for Coil B are also shown, as an example.

Clearly, the slope of the J-R curve for Pipe X is higher than Pipe Y, while slope for Coil A > Coil B (Fig. 2 (a)). The load vs CMOD plot for Coil B in H_2 shows drop in load after reaching maximum while no significant load drop is noticed in air. It clearly shows the influence of hydrogen on crack initiation and propagation. More insights based on these fracture toughness results and J-R curves, in correlation to fractography and microstructure will be presented in the following sections.

3.3. Fractography

Fractography was performed on the fracture toughness tested samples for the investigation of the fracture mode in these materials. The stretch zone associated with the crack initiation process and the extension zone associated with the crack propagation were investigated, lying in the crack plane while progressing through the longitudinal cross-section of the material. Fig. 3 shows stereo and depth field images of the fracture surface for Pipe X, tested in H_2 (100 bar). Fracture surface mapping was performed along the primary crack direction (also rolling direction) while rastering from left to right in the crack plane.

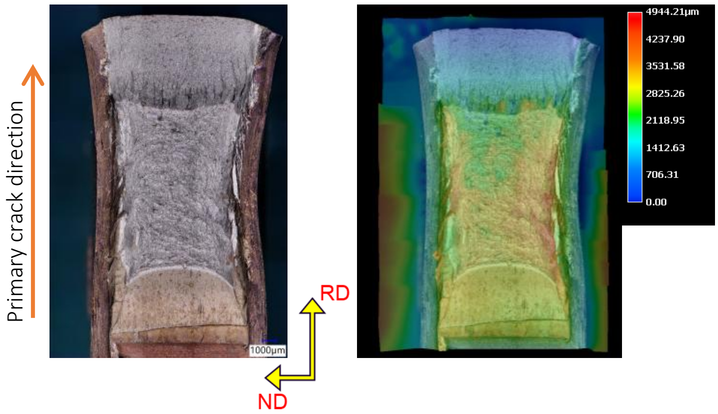

Fig. 3: Stereo and depth field image (top view) of the Pipe X fracture surface.

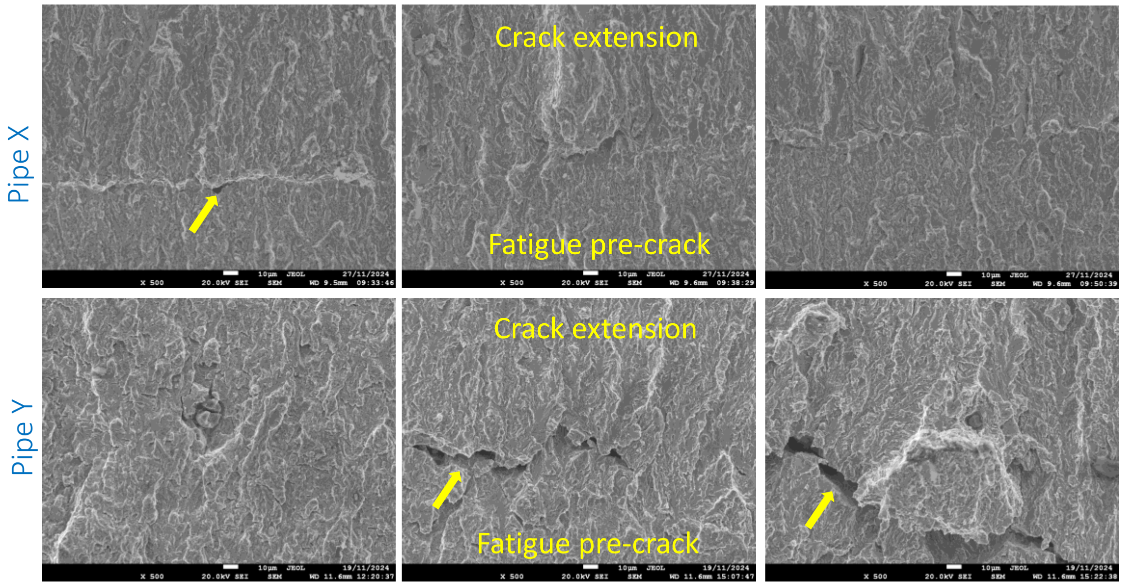

Fig. 4: Fracture surface mapping of fatigue pre-crack and crack extension interface in Pipes X and Y.

A comparison of the stretch zone at the interface of fatigue pre-crack and crack extension, between Pipe X and Pipe Y is shown in Fig. 4. In both the cases, the presence of stretch is diminished into a boundary due to the influence of hydrogen. A planar transition at the intersection of fatigue pre-crack and crack extension occurs in the direction of primary crack propagation in case of Pipe X. Some fine out-of-plane "secondary cracks" can also be observed in the stretch zone (or stretch boundary). On the other hand, the stretch zone in the case of Pipe Y is entirely flat with large secondary cracks (perpendicular to the primary crack plane & direction) marked by yellow arrows, showing the severity of failure. However, the crack extension zone is not significantly different between the two cases (Fig. 5). The morphology of the crack extension is primarily "quasi-cleavage". Several out-of-plane secondary cracks (marked by yellow arrows) are observed. In addition to the secondary cracks, some split type cracks (parallel to the primary direction), marked by green arrows are also observed (Fig. 5). Inclusions are seen to be associated with the split cracks. Indication of inclusions (complex oxide, oxysulfide) linked with the split type cracking (Fig. 6) from energy-dispersive X-ray spectroscopy (EDS).

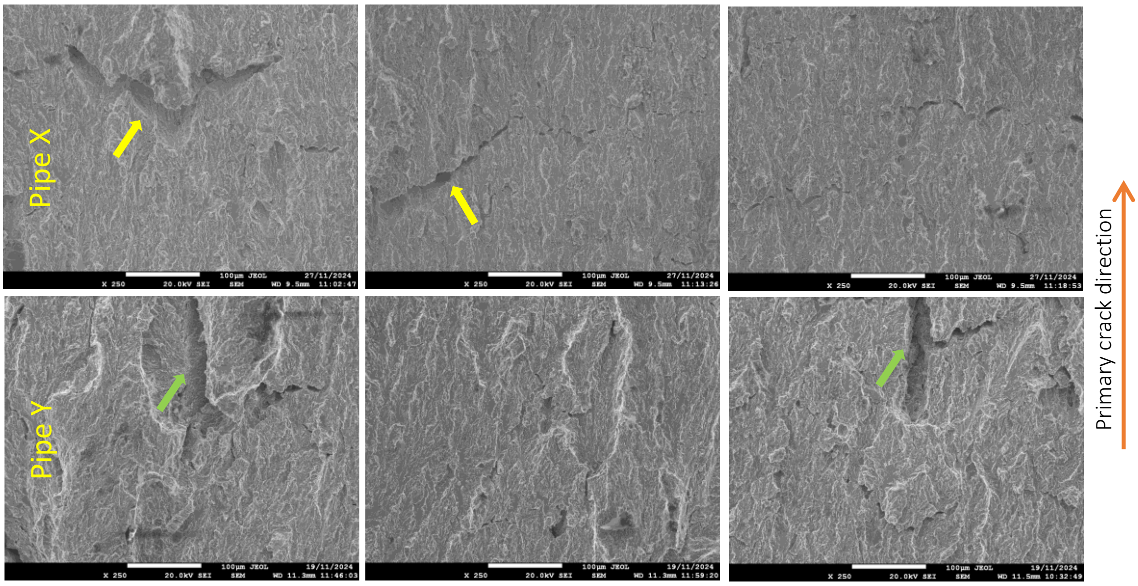

Fig. 5: Comparison of crack extension zones in Pipe X and Pipe Y, at 250x magnification.

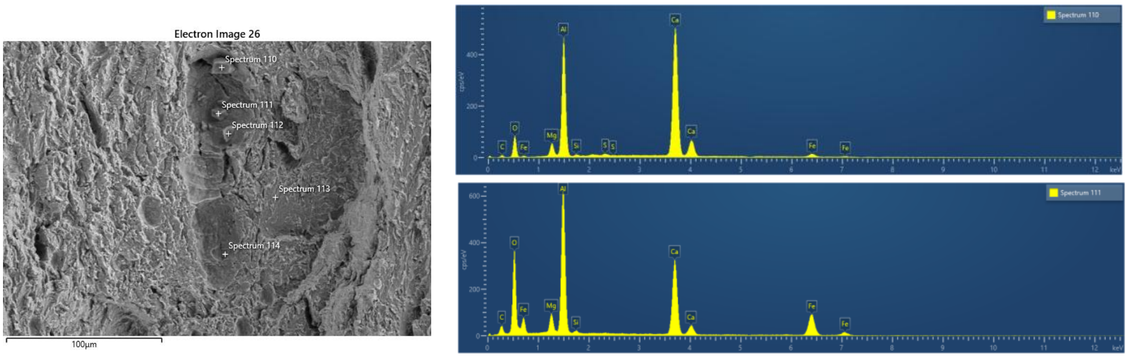

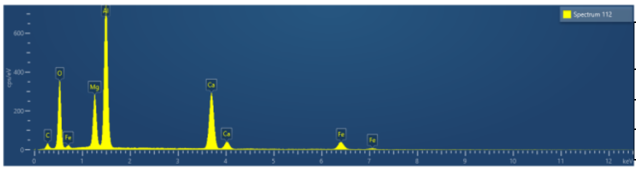

Spec-trum	C	O	Mg	Al	Si	S	Ca
110	3.87	32.58	2.52	20.9	0.29	0.35	36.7
111	11.2	44.55	2.64	17.62	0.31	--	13.28
112	9.68	43.91	7.95	21.93	--	--	12.25

Fig. 6: Electron dispersive spectroscopy (EDS) of inclusions associated with split cracks.

Similar comparisons were made between the coils, Coil A and Coil B, as shown in Fig. 7. The stretch zone (or stretch boundary) in case of Coil A is seen to be flat containing fine secondary cracks. The stretch boundary for Coil B appears to be marked by the presence of significantly large secondary cracks (marked by yellow arrows) showing the severity of fracture associated with the crack initiation process. A clear difference in morphology can be noticed between Coil A and Coil B, in the crack extension zone (Fig. 8). The crack plane morphology is primarily quasi-cleavage with out of plane secondary cracks for Coil A while “groove” or large size split cracks (marked by red arrows) running parallel to the direction of the primary crack is predominant in the case of Coil B. These significantly large size split cracks are only seen in the case of Coil B. However, these morphologies and cracks are only pertinent to 100 bar H_2 tests. The morphology is entirely different when compared to the air tested samples. An example is shown here taking the case of Coil B (Fig. 9). The morphology in the stretch boundary and crack extension zone is primarily ductile-dimple morphologies being present throughout the crack plane. Also, no out-of-plane secondary cracks or split cracks are observed. Thus, it can be concluded that these cracks are related to hydrogen induced fracture. The origin of these cracks is further investigated to shed light on the mechanistic insights in the following section.

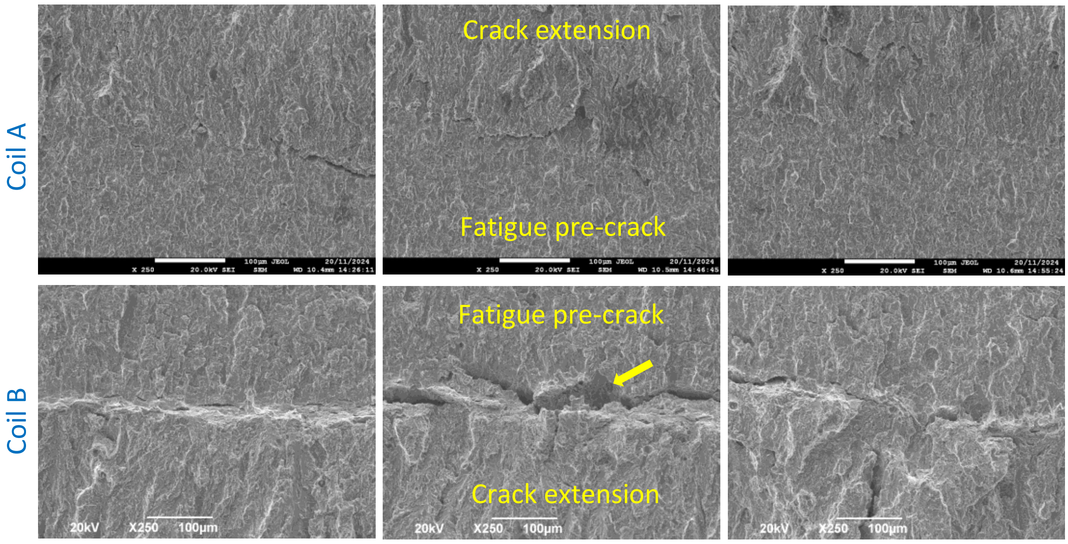

Fig. 7: Comparison of stretch zones between Coil A and Coil B, at 250x magnification.

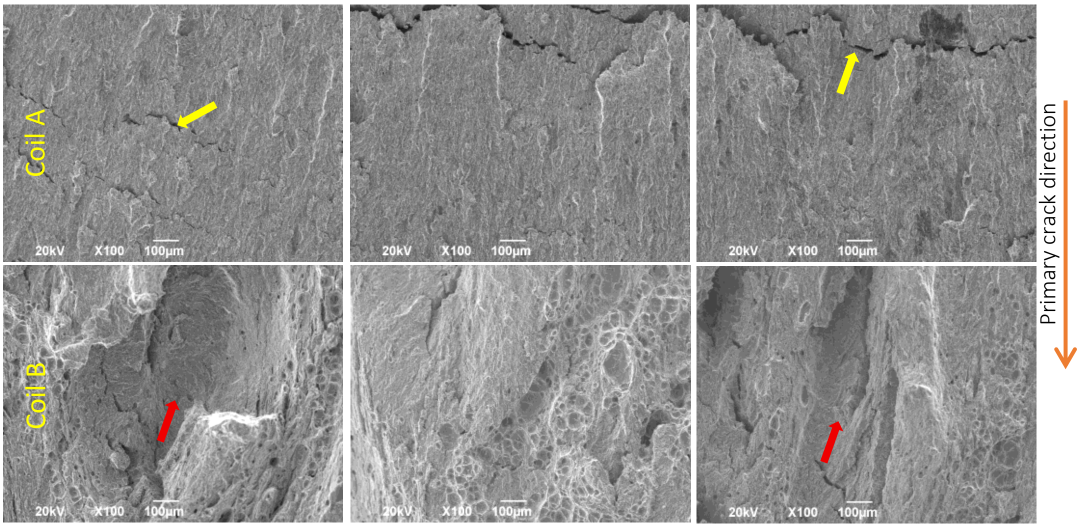

Fig. 8: Comparison of crack extension zones between Coil A and Coil B, at 100x magnification.

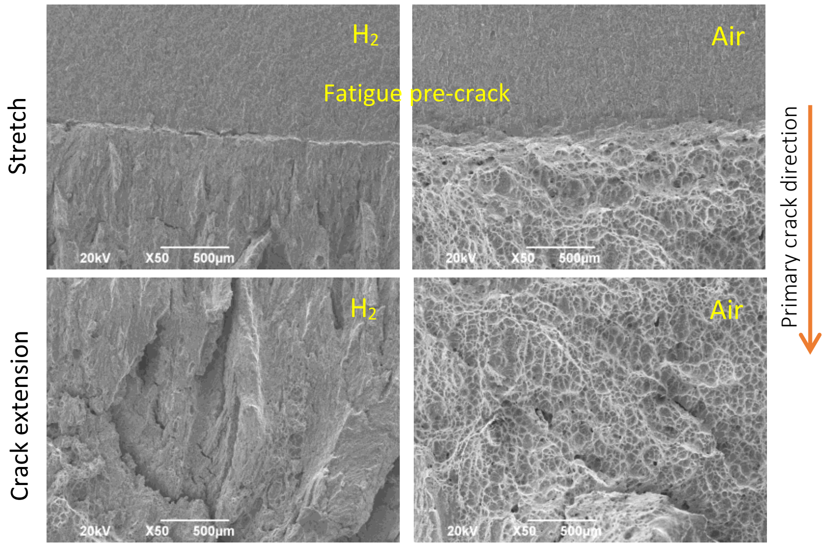

Fig. 9: Difference in morphology between the air tested and 100 bar H_2 bar fracture surfaces in the stretch and crack extension zones for Coil B, at 50x.

4. DISCUSSION

The fracture surface mapping provides a comprehensive overview of the crack initiation and propagation characteristics of these industrial grade line-pipe steels during high-pressure fracture toughness testing in H_2. The fracture morphologies in the environmental tests are significantly different from that in air. Several forms of crack branching are noticed from the primary crack plane. For instance, out-of-plane "secondary cracks" perpendicular to the primary crack direction (also rolling direction) and "groove cracks" or large split cracks parallel to the primary crack are observed from the environmental tests. The groove cracks are more exclusive to the Coil B material. Such grooves can be associated with aligned microstructural features such as segregation bands, banded structures with weak phase boundaries, non-metallic inclusions (NMIs), and crystallographic texture [9][10]. But segregation bands and banded structures were not observed in the evaluated material. Notably, Coil B exhibits a higher inclusion index, indicating a greater susceptibility to hydrogen-assisted cracking at weak inclusion/matrix interfaces. Crystallographic texture also plays a significant role, as delamination tends to follow brittle {001} planes. When these planes are aligned parallel to the splitting direction, they can serve as preferential paths for crack propagation. Hydrogen can further weaken these planes through hydrogen-enhanced decohesion (HEDE) [11], promoting the formation and growth of groove-like cracks. Such groove cracks were absent in samples tested in air, underscoring the critical role of hydrogen in their development. In fact, the fracture toughness drop for Coil B in H_2 is one of the highest compared to its air counterpart (Table 2), showing the significant deleterious impact of hydrogen on material behaviour. Further investigations are required to fully understand the mechanisms at play in the current context.

The origin of the out-of-plane "secondary cracks" perpendicular to the primary crack direction is rather mysterious and somewhat unique. Unlike the grooves, no microstructural feature, such as, inclusions, banded microstructure etc. could be directly linked to these secondary cracks. As a result, further investigation was carried out leveraging advanced characterization techniques considering Pipe Y as an example case. For this purpose, samples (<200 nm thickness) were machined using the focused ion beam (FIB) technique from stretch zone in the fracture surface of Pipe Y, for transmission electron microscopy (TEM) and electron backscattered diffraction (EBSD). The FIB lamella was lifted in the vicinity of the stretch boundary by welding a secondary crack with Pt deposition to preserve the crack. Following the Pt welding, Pt deposition was carried out to preserve the surface of interest oriented in the primary crack direction (RD) for FIB machining. The FIB lamella was then used for imaging using TEM. Earlier researchers have used the duo FIB and TEM to study the local microstructural evolution beneath the fracture from the fatigue tests of a ferritic-pearlitic low carbon steel in H_2 [12]. In this research, the application of that technique has been extended to study the origin of the secondary cracks generated during the fracture toughness tests. Refined microstructural features are observed around the secondary crack area from TEM characterization as shown in Fig. 10. These microstructural features could be identified as dislocation cells. The dislocation cells comprise of dislocations surrounded by low angle dislocation cell boundaries (marked by red arrows in Fig. 10) that are generated due to excessive accumulation of dislocations. The low angular misorientation (< 2°) of the dislocation cell boundaries was further confirmed from transmission Kikuchi diffraction (TKD) combined with kernel angular misorientation (KAM). Observation of similar dislocation cells underneath the fracture surface were earlier reported from fatigue tests in H_2 and is related to hydrogen enhanced localized plasticity (HELP) mechanism [12]. Needless to mention, the cyclic loading from the fatigue test is different from the nature of loading during a fracture toughness test. However, the secondary crack formations, somewhat unique to the current observations could rise from hydrogen mediated fracture. It can be hypothesized that higher hydrogen concentration local to the primary crack-tip driven by stress triaxiality and anisotropy, could lead to these secondary crack formations. The fact that they are related to hydrogen can be asserted from the observation of the dislocation cells in the vicinity of the secondary crack (Fig. 10). Following the HELP mechanism [13], it can be stated that hydrogen enhanced dislocation mobility and rapid accumulation resulted in localized plasticity and softening ultimately leading to the secondary crack formation. It is also possible that alongside HELP, multiple mechanisms are at play, such as, adsorption-induced dislocation emission (AIDE) [14] and HEDE. However, their possible role and involvement will be investigated further.

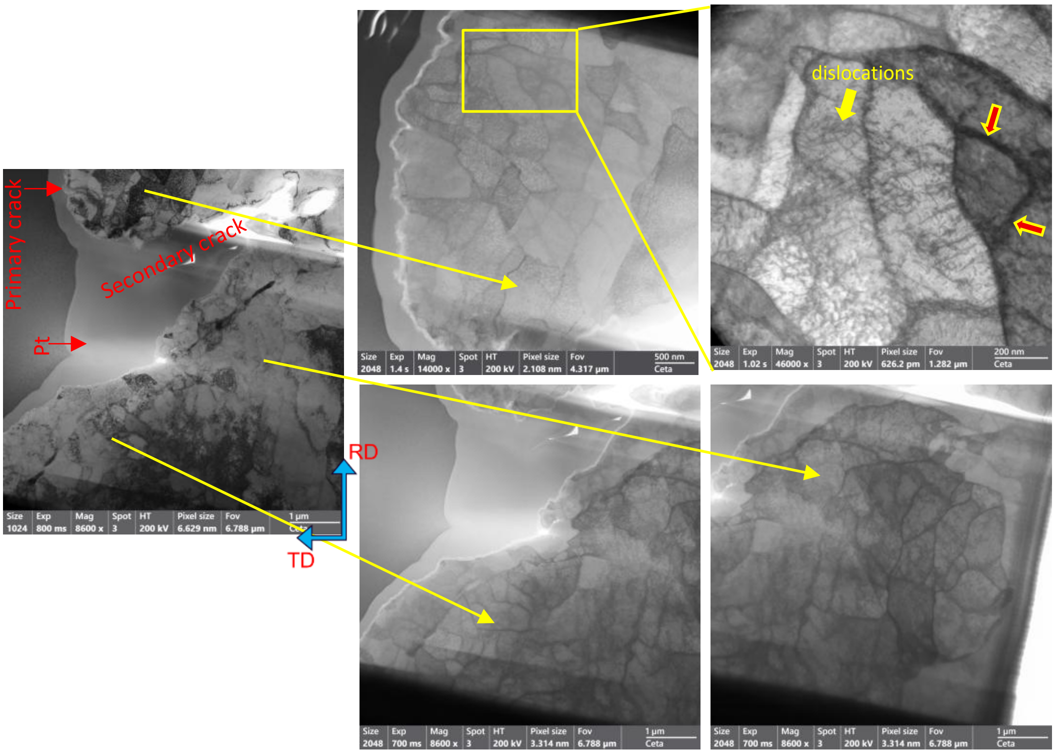

Fig. 10: TEM images of the FIB lamella showing dislocation cells in Pipe Y tested at 100 bar H_2.

The role of hydrogen leading to these secondary cracks are further confirmed from the TEM characterization of another FIB lamella from the fracture surface of an air tested Pipe Y sample. Similar to the H_2 tested case, the FIB lift-out was performed close to the stretch boundary (from the fracture surface). However, no such dislocation cell formation was observed (Fig. 11). The grains appear to be elongated (or stretched) and somewhat deformed in the thickness (or normal) direction. A clear difference in the grain morphology can be noticed just close to the fracture surface compared to those which are a few hundred microns away as shown in Fig. 11. Such morphology underneath the fracture surface could be related to the shearing of the grains during crack initiation and propagation, which are a sign of ductile fracture experienced by the material in air. The difference in morphology just beneath the fracture surface between the air and environment tested cases further confirms the mechanistic insights on hydrogen mediated secondary crack formation during the environmental test. Thus, the role of hydrogen in generating the secondary cracks along with the associated mechanisms for such crack formation is explained. As far as the primary crack is concerned, multiple FIB lift-outs and TEM were performed to study the microstructural evolution just beneath the crack plane. Some dislocation cell structures were observed but no dense network was seen while comparing to the secondary crack case (Fig. 10). The primary crack initiation and propagation could be due to multiple mechanisms acting together, i.e., HEDE and HELP. The predominant quasi-cleavage morphologies observed from the fracture surface mapping could be a manifestation of HEDE. The interplay and switch between mechanisms (HEDE and HELP) is dependant on the hydrogen concentration distribution. Since the primary crack is directly exposed to H_2, a higher hydrogen concentration at the primary crack tip is possible due to higher hydrostatic stress and direct absorption followed by adsorption. And HEDE is preferred for a higher hydrogen concentration. On the other side, stress triaxiality along with anisotropy ahead of the crack tip could lead to preferential hydrogen accumulation locally (in lower amount relative to the primary crack plane) along certain locations perpendicular to the crack plane leading to these secondary crack formations manifested through HELP.

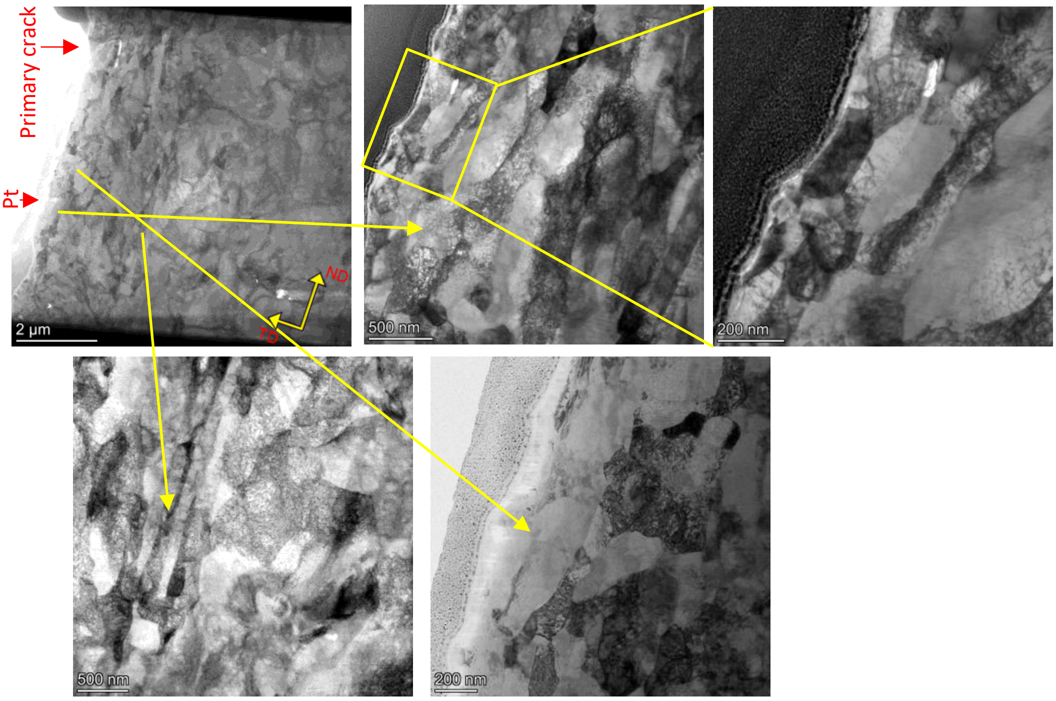

Fig. 11. TEM images of the FIB lamella showing dislocation cells in Pipe Y tested in air.

Additional efforts were made to quantify the secondary cracks observed in the stretch and crack extension zones using a computer vision approach. An algorithm was developed to assess the amount (area fraction) of cracks and their direction from the images. By using Gabor kernels to filter the images sharp darker areas in the image can be located. In this proof of concept, Gabor kernels with orientations 0 and 90 degrees are used (Fig 12). The Gabor filtering also picks up unrelated specks in the image, in addition to cracks. These constitute a noise on the signal and thus measures were taken to filter those out based on neighbouring pixel contrast. The crack areas usually follow a log-normal distribution, and the specks can be identified as outliers on the lower end of the distribution spectrum to be filtered out using a low-end cut-off filter. The result is denoted as 'filtered' for the corresponding cases (Fig. 13). It should be noted that this method is a proof of concept and will be refined further. And from those quantifications, it can be observed that Pipe Y has higher area fraction of secondary cracks compared to the Pipe X. This observation also corresponds to the slope of the J-R curves (Fig. 2), where slope of Pipe X > Pipe Y. Thus, it can be stated that higher secondary crack formation leads to lower crack initiation and growth resistance in H_2. But the secondary cracks are less detrimental when compared to the "groove cracks" as can be reasoned while comparing Coil A and Coil B. Coil A with only secondary cracks shows higher crack initiation and eventually higher crack growth resistance than Coil B (with grooves) as corroborated from the higher fracture toughness and J-R curve slope for Coil A (Fig. 2). The primary crack branching leads to secondary crack formation in H_2 environments could contribute to higher energy absorption. However, more investigation is necessary in this direction.

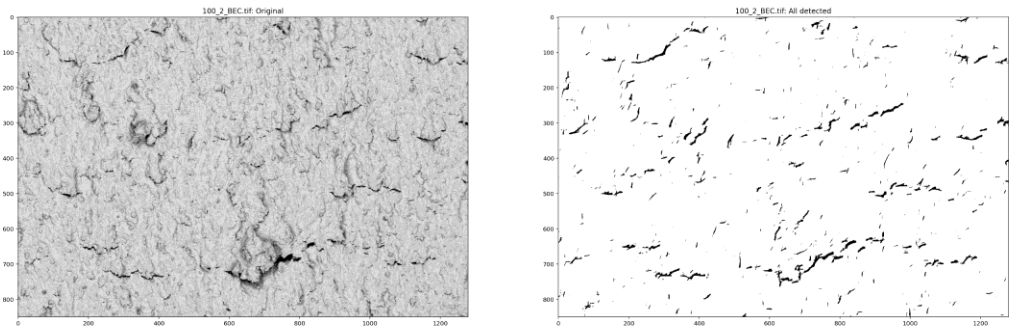

Fig. 12. Binary converted image from BSE fracture surface image using Gabor filtering.

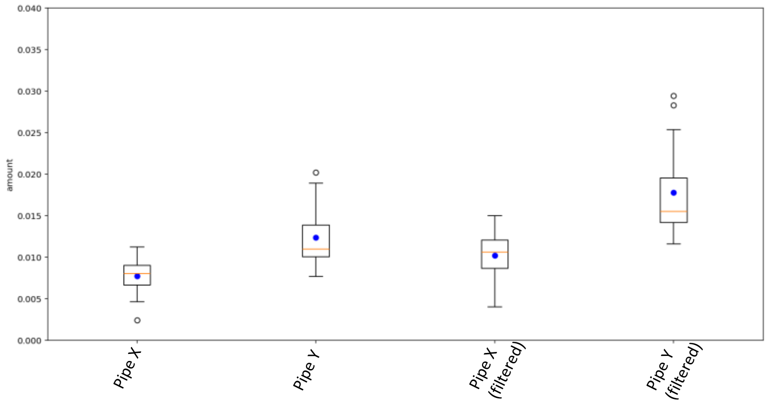

Fig. 13: Area fraction (amount) of secondary cracks for Pipe X and Pipe Y using computer vision.

5. CONCLUSIONS

The research summarizes the relative fracture toughness performances of a pair of coils and pipes in 100 bar H_2 environment. Their fracture toughness performance was understood based on a comprehensive postmortem analysis combining fracture surface mapping and advance characterization of microstructural evolution just beneath the fracture surface, shedding light on the HE mechanisms. Evaluations from this research could also contribute towards the development of a dedicated environmental test methodology for H_2 applications. Some of the important conclusions are as follows:

1. Fracture toughness tests in H_2 corresponds to the trend observed from the in-situ SSRT tests (with electrochemical charging) reinforcing the conclusion that steel cleanliness influences line-pipe steel susceptibility to HE.
2. Fractography shows out-of-plane secondary crack formation perpendicular to the primary crack direction in the coils and pipes in 100 bar H_2 except for Coil B. Large split cracks (delamination), i.e., the "groove cracks" are only seen in the crack plane of Coil B. A good correlation was observed between fracture toughness results and fracture modes and morphologies. Pipe Y and Coil B with lower fracture toughness exhibit more large-size secondary cracks at the stretch zone (boundary) compared to Pipe X and Coil A, respectively.
3. The secondary cracks are a result of hydrogen mediated fracture. High density of dislocation cell formation with localized dislocation accumulation observed along the secondary crack area in FIB lamella from the fracture surface. Indications of HELP leading to secondary crack formation.
4. Machine learning technique rooted in computer vision indicates lower crack growth resistance in H_2 could be associated with more secondary crack formations.

6. ACKNOWLEDGEMENTS

The authors would like to acknowledge Davit Melkonyan and Vahid Samaee, research engineers at ArcelorMittal Global R & D Gent (OCAS), for their contribution with FIB and TEM characterization.

7. REFERENCES

[1] Global Hydrogen Review 2024, International Energy Agency.
[2] Topolski K, Reznicek EP, Erdener BC, San Marchi CW, Ronevich JA, Fring L, Simmons K, Fernandez OJ, Hodge BM, Chung M. (2022): Hydrogen blending into natural gas pipeline infrastructure: Review of the state of technology.
[3] Stalheim D, Slifka A, Uranga P, Kang DH, Lucon E (2020): Cross-Sectional Grain Size Homogeneity Effect on Structural Steel Fatigue Performance in Air and Hydrogen Environments IPC2020-84461. International Pipeline Conference 2020, Calgary, Alberta. ASME, New York
[4] ASTM E1820-22: Standard Test Method for Measurement of Fracture Toughness, American Society for Testing and Materials, 2022.
[5] CSA CHMC 1-2014, Canadian Standards Association, 2014.
[6] ISO 4967, Determination of content of nonmetallic inclusions, International Standardization Organization, 2013

[7] ASME B31.12-2019, Hydrogen Piping and Pipelines: ASME Code for Pressure Piping, American Society of Mechanical Engineers, 2019.
[8] Mechanical Testing Phase 1, H2PIPE JIP - Design and Operation of Hydrogen Pipelines, DNV, 2023.
[9] Tankoua F (2015): Ductile to brittle transition in pipeline steels: Quantitative Investigation of Brittle Out-of-Plane Cracking and Correlation to Microtexture Anisotropy (Doctoral dissertation, Sciences des Métiers de L'Ingénieur, L'École Nationale Supérieure des Mines de Paris).
[10] Gervasyev A, Pyshmintsev I, Petrov R, Huo C, Barbaro F (2020): Splitting susceptibility in modern X80 pipeline steels. Materials Science and Engineering: A, 772, p.138746.
[11] Katzarov IH, Paxton AT (2017): Hydrogen embrittlement II. Analysis of hydrogen-enhanced decohesion across (111) planes in α-Fe. Physical Review Materials, 1(3), p.033603.
[12] Wang S, Nagao A, Sofronis P, Robertson IM (2018): Hydrogen-modified dislocation structures in a cyclically deformed ferritic-pearlitic low carbon steel. Acta Materialia, 144, pp.164-176.
[13] Robertson IM (1999): The effect of hydrogen on dislocation dynamics. Engineering fracture mechanics, 64(5), pp.649-673.
[14] Lynch S (2012): Hydrogen embrittlement phenomena and mechanisms. Corrosion reviews, 30(3-4), pp.105-23.